Programmable Viscoelasticity in Protein-RNA Condensates with Disordered Sticker-Spacer Polypeptides

Ibraheem Alshareedah*, Mahdi Muhammad Moosa, and Priya R. Banerjee*

Department of Physics, University at Buffalo, Buffalo NY 14260, USA

*All correspondence could be addressed to:

Priya R. Banerjee (email: prbanerj@buffalo.edu)

Ibraheem Alshareedah (email: ialshare@buffalo.edu)

The rheological properties of biological matters play a fundamental role in many cell processes. At the organelle level, liquid-liquid phase separation of multivalent proteins and RNAs drives the formation of biomolecular condensates that facilitate dynamic compartmentalization of cellular biochemistry[1]. With recent advances, it is becoming increasingly clear that the structure and rheological properties of these condensates are critical to their cellular functions[2,3]. Meanwhile, aberrant liquid-to-solid transitions in some cellular condensates are implicated in neurodegenerative disorders[4]. Within the limits of two extreme material states, viz., viscous liquid and amorphous or fibrillar solid, there lies a spectrum of materials known as viscoelastic fluids. Viscoelastic fluids behave as an elastic solid at time-scales shorter than their network reconfiguration time but as a viscous fluid at longer time-scales. Viscoelasticity of biomolecular condensates may constitute an adaptive mechanism for sensing mechanical stress and regulating biochemical processes[5]. From an engineering standpoint, viscoelastic fluids hold great potential for designing soft biomaterials with programmable mechanosensitivity[6,7]. Here, employing microrheology with optical tweezers, we demonstrate how multivalent disordered sticker-spacer[8,9] polypeptides undergoing associative phase separation with RNA can be designed to control the frequency-dependent viscoelastic behavior of their condensates. Utilizing linear repeat polypeptides inspired by natural RNA-binding sequences, we show that polypeptide-RNA condensates behave as Maxwell fluids, with viscoelastic behavior that can be fine-tuned by the identity of the sticker and spacer residues. The sequence heuristics that we uncovered allowed us to create biomolecular condensates spanning two orders of magnitude in their viscous and elastic responses to the applied mechanical stress. This sequence-encoded regulation of viscoelasticity in disordered polypeptide-RNA condensates establishes a link between the molecular architecture of the polypeptide chains and the rheological properties of the resulting condensates at the mesoscale, enabling a route to engineer soft biomaterials with programmable mechanics.

Biomolecular condensates formed by multivalent proteins display a wide range of material properties from dense liquids to viscoelastic fluids and amorphous/ fibrillar solids[1,9,10]. Multivalency in a protein chain is typically encoded either by intrinsically disordered regions (IDRs) with repeated amino acid sequences (such as the Arg−Gly−Gly or RGG repeats) or by folded domains (such as SH_3 and PRM modules) or a combination thereof[9]. Multivalent homotypic protein-protein and heterotypic protein-RNA interactions driving biomolecular condensation have been elegantly described by the stickers-and-spacers polymer framework[8,9,11,12]. For IDRs, the residues that primarily enable inter-chain interactions, such as arginine (R) in R/G-rich IDRs and tyrosine (Y) in prion-like IDRs, are usually considered as “stickers”[13]. Additionally, the linker residues connecting these stickers are considered as “spacers”. The sequence composition and patterning of stickers and spacers can alter the physical properties of condensates and their phase behavior[13,14]. Therefore, understanding how the sticker-spacer architecture of disordered protein chains can be harnessed to create condensates with programmable material properties, as found in biological systems, is of interest for understanding biological mechanisms and designing novel biomaterials.

Establishing a molecular grammar of sequence-encoded protein-protein and protein-RNA interactions that governs the biomolecular condensate dynamical properties requires systematic measurements of the frequency-dependent viscous and elastic moduli of the condensate[9]. The linear viscoelastic (LVE) behavior of homotypic protein condensates has recently been studied by active oscillatory microrheology using a dual-trap optical tweezer[5,15]. However, passive non-

oscillatory measurements using a single optical trap offers an attractive orthogonal route to probe the LVE properties of complex fluids over a wide range of experimentally accessible frequencies[16,17]. Passive microrheology with optical tweezers (pMOT) only requires a single optical trap and does not need independent calibration measurements[18-21], making it convenient and well-suited for relatively high throughput studies. Here, we employ in-droplet pMOT to map the sequence-encoded and frequency-dependent viscoelastic properties of polypeptide-RNA condensates *in vitro* over 3 decades of frequency from a single measurement. Briefly, 1 μm polystyrene beads are passively embedded within a condensate (placed on a glass surface) with each condensate containing at least one probe particle (Fig. 1a). The bead is constrained within the condensate by an optical trap (Fig. 1b). The motion of the bead inside the condensate is driven by the thermal fluctuations of the medium (the condensate) and constrained by the harmonic potential of the optical trap (Fig. 1c). The complex modulus of the condensate can be calculated from the normalized position autocorrelation function of the bead $A(\tau)$ and the trap stiffness κ as[18,20]

$$G^*(\omega) = \frac{\kappa}{6\pi a}\left(\frac{i\omega\hat{A}(\omega)}{1-i\omega\hat{A}(\omega)}\right) = G'(\omega) + iG''(\omega) \quad (1)$$

Where a is the bead radius and $\hat{A}(\omega)$ is the Fourier transform of $A(\tau)$ (see Methods for details). In equation (1), G' and G'' represent the elastic and viscous modulus of the condensate, respectively. Using pMOT, we first measured the frequency-dependent viscoelastic moduli of a model peptide-RNA condensate formed by a short disordered lysine-rich repeat peptide $[KGKGG]_5$ and a homopolymeric RNA $[rU]_{40}$ (rU40) (Fig. 1a). We found that $[KGKGG]_5$-rU40 condensates display a complex modulus that is dominated by the viscous component (G'') at both low and high frequencies (0.1 to 100 Hz), indicating a predominant liquid-like behavior (Fig. 1d&e). The zero-shear viscosity (η) of $[KGKGG]_5$-rU40 condensates, which is directly obtained from the slope of the viscous modulus ($\eta = G'/\omega$), is ~ 0.27±0.05 Pa.s. This is ~ 300-fold higher than the viscosity of water and is nearly-independent of the frequency (Fig. 1e), suggesting that these condensates behave mostly as a viscous liquid throughout the entire experimentally accessible frequency range. To cross-validate our results obtained from pMOT, we independently measured the viscosity of $[KGKGG]_5$-rU40 condensates using video particle tracking (VPT)-based microrheology[22] and found good agreement (Fig. 1f&g). Therefore, pMOT presents a suitable method to probe the frequency-dependent LVE properties of protein-RNA condensates (see Methods).

A significant fraction of eukaryotic ribonucleoproteins (RNPs) contains Arginine/Glycine-rich IDRs[23,24] as RNA-binding motifs. Arginines in R/G-rich IDRs are classified as "stickers" that potentiate RNP phase separation with RNA through a combination of electrostatic, cation-π and π-π interactions[25,26]. Due to their multivalent architecture, the R/G-rich IDRs have the potential to serve as programmable stickers-and-spacers polypeptides with tunable condensation behavior with RNA (Fig. 2a). To test this, we designed a synthetic repeat polypeptide encompassing 5 repeats of RGRGG, $[RGRGG]_5$. pMOT experiments on $[RGRGG]_5$-rU40 condensates revealed dominant elastic behavior at high frequencies (short-time scales) and viscous behavior at low frequencies (long-time scales). This frequency-dependent mechanical behavior of R/G condensates is reminiscent of a typical Maxwell fluid[18] (Fig. 2b) with a single crossover frequency between the elastic and the viscous regimes. This crossover frequency is the inverse of the terminal relaxation time (τ_M) of the condensate network (Fig. 2b), which signifies the average peptide-RNA network reconfiguration time[16]. For $[RGRGG]_5$-rU40 condensates, τ_M is 60±10 ms,

meaning that in time-scales shorter than 60 ms, the $[RGRGG]_5$-rU40 condensates behave as an elastic solid (with G'>G'') and vice-versa (Fig. 2b). This is in stark contrast with $[KGKGG]_5$-rU40 condensates which behave as a predominantly viscous liquid (Fig. 1e) within the same frequency range (0.1 to 100 Hz). Consistent with this observation, the zero-shear viscosity of R/G-rU40 condensates is ~ 4±1 Pa.s (Fig. S1), which is ~ 15-fold higher than the same for K/G-rU40 condensates. This difference in viscosity between R/G and K/G condensates is consistent with previously published reports[14,25,27] and signifies a broad range of accessible dynamical properties in these condensates based on the choice of stickers (*i.e.,* Arg *vs.* Lys).

Besides Arg and Gly residues, R/G-rich domains in natural RNPs frequently contain aromatic and polar residues[28]. Our bioinformatics analysis of RG/RGG motifs from > 400 human RNA-binding proteins[29] reveal that R/G-rich IDRs are primarily interspersed with four uncharged amino acids: Tyrosine (Y), Phenylalanine (F), Serine (S), and/ or Proline (P) (Fig. 2c). The occurrence of these four residues within R/G-rich IDRs can be important for modulating self-interactions and interactions with RNA and/ or the solvent. As such, these sequence variations may control the material properties of polypeptide-RNA condensates. To test this idea systematically, we designed a variable sticker-spacer polypeptide sequence, $[RG\underline{X}GG]_5$, where the amino-acid X can be Y, F, S, P, or R (Table S1). In the context of our work, amino acids, such as R or K, that primarily contribute to the RNA binding are defined as stickers, while spacers are linker residues connecting the stickers, such as G. Employing our pMOT assay on condensates formed by $[RG\underline{X}GG]_5$ and rU40 RNA (Fig. S2), we found a rich variation in the viscoelastic behavior that spans two orders of magnitude depending on the identity of the amino acid $\underline{X}$. In discussing these results, we choose $[RGRGG]_5$ as our reference system (X = Arg). Setting X = Phe, we observed a 2-fold increase in the terminal relaxation time from 60±10 ms to 110±40 ms, and ~2-fold increase in the zero-shear viscosity of peptide-rU40 condensates (Fig. 2d-f). Intriguingly, setting X = Tyr resulted in condensates that exhibited an order of magnitude increase in both the terminal relaxation time (~ 900±400 ms, Fig. 2d&e) and the zero-shear viscosity (~ 40±10 Pa.s, Fig. 2e&f & Fig. S3). The frequency-dependent viscoelastic moduli of both $[RGYGG]_5$ and $[RGFGG]_5$ condensates are well described by a Jeffrey fluid model, which represents a linear combination of a Maxwell fluid and a Newtonian fluid[5,30] (Fig. 2d). The high terminal relaxation time for $[RG\underline{Y}GG]_5$-rU40 condensates ($\tau_M \sim 0.9$ s) indicates that these condensates are dominantly elastic over a much longer time-scale than $[RGRGG]_5$-rU40 and $[RGFGG]_5$-rU40 condensates ($\tau_M \sim 0.06$ s, Fig. 2g). This is consistent with the fact that Tyrosine residues are stronger drivers of phase separation as compared to Phenylalanine[13,14]. In the context of known biological assemblies, the observed LVE behavior of $[RG\underline{Y}GG]_5$-rU40 condensate is comparable to that of the reconstituted extracellular matrix[7].

To independently verify the difference in the dynamical properties between $[KGKGG]_5$, $[RGRGG]_5$, and $[RGYGG]_5$ condensates (Fig. S2), we employed an active microrheology experiment through flipping optical traps[19] (see Methods). This experiment is a micro-scale adaptation of step-strain experiments typically utilized in bulk rheological studies[17,19]. Here, the optical trap holding a polystyrene bead within a condensate is shifted instantaneously to a location that is ~ 0.3 μm away from the center of the bead (Fig. 2h). The time-scale at which the bead follows the optical trap is determined by the strength of the optical trap and the dynamical properties of the condensate. Under similar experimental conditions, we find that the bead takes ~ 95±2 ms to return to the center of the optical trap for $[RGRGG]_5$-rU40 and ~ 1880±4 ms for $[RGYGG]_5$-rU40 condensates whereas the process happens almost instantaneously for $[KGKGG]_5$-rU40 condensates (8.8±0.9 ms, comparable to the experimental dead time; see

Methods; Fig. 2i). Consistent with these results, VPT experiments of free polystyrene beads[22] (without optical traps) revealed two diffusion modes for [RGYGG]$_5$-rU40 condensates, representing clearly distinguishable elastic and viscous regimes (Fig. 2j). The first mode at short time-scales displayed a constant MSD as a function of time, whereas a transition to a linear diffusion ($MSD = 4D\tau$) was observed at ~1200 ms time-scale. This is consistent with the terminal relaxation time obtained from pMOT (900±400 ms) (Fig. 2d&e).

Contrary to X = Tyr or Phe, setting X = Pro or Ser resulted in a complete loss of elasticity across the tested frequencies (Fig. 2d) akin to the [KGKGG]$_5$-rU40 condensates. The zero-shear viscosity of [RGPGG]$_5$-rU40 condensates was ~0.19±0.08 Pa.s, which is ~ 20-fold lower than the [RGRGG]$_5$-rU40 condensates (Fig. 2f) and ~200 fold lower than the [RGYGG]$_5$-rU40 condensates. Similarly, the viscosity of [RGSGG]$_5$-rU40 condensates was found to be 0.42± 0.06 Pa.s. Taken together, our bioinformatics-guided sticker-spacer peptide designs reveal that tyrosine, phenylalanine, and arginine are promoters of elasticity in R/G-repeat polypeptide-RNA condensates, while lysine, proline, and serine residues promote the formation of predominantly viscous condensates (Fig. 2g, Fig. S3, and Table S2).

In addition to stickers, spacer residues may also impact the condensate dynamical properties[12]. To explore such an effect, we designed a generic polypeptide [RxRxx]$_5$ where x can be either glycine, glutamine, alanine, proline, or leucine (G, Q, A, P, or L, respectively). We observed that G-to-P substitutions reduced the condensate viscosity by an order of magnitude (Fig. 3a-c) and resulted in at least an order of magnitude lower relaxation time (τ_M ~10 ms since the crossover is slightly beyond the experimental frequency range, Fig. 3a). However, [RPRPP]$_5$-rU40 still showed a higher zero-shear viscosity (~1.3±0.2 Pa.s) as compared to [RGPGG]$_5$ (~0.19±0.08 Pa.s, Fig. 2f), which indicates that replacing arginine (i.e., “stickers”) residues with proline directly impacts the peptide-RNA interactions and results in larger effects on the condensate rheological properties. For RQRQQ repeats, we also found a reduced viscosity and relatively weaker elastic component than [RGRGG]$_5$-rU40 condensates (Tables S1&S2 and Fig. 3a-c). In contrast, [RARAA]$_5$-rU40 condensates showed a comparable elastic response (τ_M = 50±20 ms) and slightly higher zero-shear viscosity (~ 6±1 Pa.s) than [RGRGG]$_5$-rU40 condensates (Fig. 3). Finally, mutating G-to-L ([RLRLL]$_5$) resulted in the formation of arrested networks instead of liquid condensates (Fig. S4) under identical experimental conditions. These results highlight that the LVE properties of peptide-RNA condensates can independently be controlled via spacer residue variation (Fig. 3), and in combination with the stickers (Fig. 2), these alterations can further attenuate or magnify the viscoelastic behavior of their condensates with RNA.

Based on our results on binary peptide-RNA condensates (Fig. 4a&b), we next considered two orthogonal strategies to fine-tune the viscoelasticity of our synthetic condensates – (a) by sequential perturbation of sticker identity in polypeptides; and (b) by mixing peptides with orthogonal LVE behavior. Based on our results showing enhanced viscoelasticity of peptide-rU40 condensates upon replacing RGRGG repeats with RGYGG repeats (Fig. 2 and Fig. 4b), we considered a sequential introduction of R-to-Y mutations in the 2nd arginine of RGRGG-repeats (Table S1). This sequence perturbation strategy led to a progressive enhancement of the viscosity (~4 to ~40 Pa.s) and the terminal relaxation time (~60 to ~900 ms) of peptide-rU40 condensates as a function of the number of R-to-Y substitutions (Fig. 4c-e and Fig. S5). In our second set of experiments, instead of a single polypeptide, we utilized a mixture of two polypeptides with orthogonal LVE behavior, viz., [RGYGG]$_5$, which forms predominantly elastic condensates, and

$[RGPGG]_5$, which forms viscous droplets with rU40 RNA (Fig. 2d and Table S2). We observed that $[RGYGG]_5$ acts as a dopant that progressively enhances the viscoelasticity of $[RGPGG]_5$ condensates with rU40(Fig. 4f-h). The ternary peptide-RNA mixtures ($[RGYGG]_5$, $[RGPGG]_5$, and rU40) formed homogeneous condensates at all mixing ratios with LVE properties that can be controlled by the molar ratio of $[RGYGG]_5$ and $[RGPGG]_5$ (Figs. S6 and S7). We observed a monotonic increase in the zero-shear viscosity (~0.19 to ~40 Pa.s) and the terminal relaxation time (~22 to ~900 ms) as a function of $[RGYGG]_5$:$[RGPGG]_5$ ratio (Fig. 4f&g). This result suggests a plausible mechanism for the regulation of the LVE properties of multi-component biomolecular condensates, where the similarity in linear sequences promotes the formation of well-mixed condensates (as opposed to multiphasic condensates[31]) and the dissimilarity in sticker identity allows for composition-dependent regulation of the condensate viscoelasticity (Fig. 4h). Taken together, our results demonstrate simple design strategies to control the mechanical behavior of biomolecular condensates formed by stickers-and-spacers polymers (Fig. 4c-h).

In conclusion, we implement an optical tweezer-based microrheology technique (pMOT) to systematically explore the frequency-dependent LVE properties of synthetic protein-RNA condensates formed by RNP-inspired sticker-spacer polypeptides. We show that R/G-repeat polypeptide-RNA condensates are Maxwell fluids, which behave as an elastic solid at short time-scales and as a viscous fluid at long time-scales. Both viscosity and the time-dependent network elasticity can be precisely controlled via polypeptide chain sequence and/or by mixing multiple polypeptide chains with distinct sticker-spacer architectures. The LVE properties of biomolecular condensates are thought to be intricately coupled to their physiological function and alterations thereof have been linked to pathological dysfunction[4,32]. Therefore, the observed tunability of the LVE behavior of peptide-RNA condensates may provide key insights into the context-dependent regulation of material properties of intracellular RNP condensates. In a broader sense, the mechanical plasticity of biological matters, such as the extracellular matrix, impacts many fundamental cellular processes[7]. Accordingly, engineered condensates formed by sticker-spacer polypeptides with programmable viscoelasticity may provide a route to regulate mechano-sensitive cell processes. Finally, the application of laser tweezer-based microrheology will pave the path for understanding the molecular origins of viscoelasticity in membrane-less organelles.

DATA AVAILABILITY

All data relevant to the findings of this manuscript are included in the manuscript and the supplementary appendix. Additional data are available from the authors upon reasonable request.

CODE AVAILABILITY

All analysis and calculations were done using custom-made python scripts that can be made available by the authors upon reasonable request.

ACKNOWLEDGEMENTS

The authors acknowledge Dr. Manlio Tassieri of the University of Glasgow, UK for valuable discussions. P.R.B. acknowledges the College of Arts and Sciences at the University at Buffalo, SUNY, and the National Institute of General Medical Sciences (NIGMS) of the National Institutes of Health (R35 GM138186) for financial support.

AUTHOR CONTRIBUTIONS

P.R.B. conceived the idea. P.R.B. and I.A. designed the study. I.A. performed the experiments and data analysis. M.M.M. performed the bioinformatics analysis. P.R.B. and I.A. wrote the manuscript with input from M.M.M.

COMPETING INTERESTS

The authors declare no competing interests.

Figures and Legends

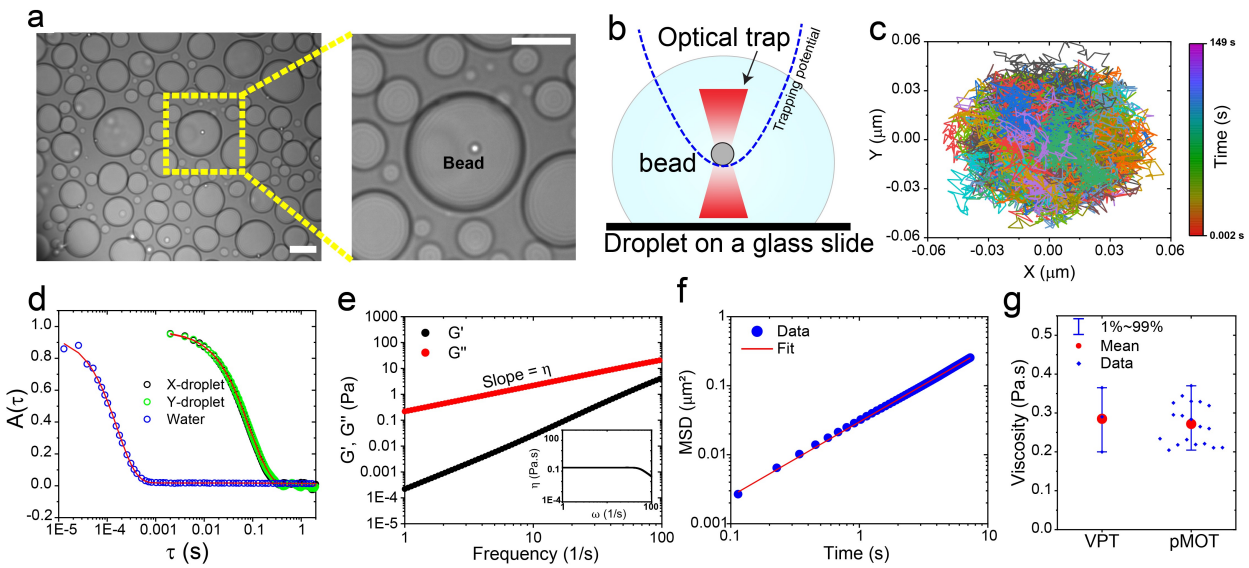

Figure 1. Determination of frequency-dependent viscoelastic moduli of peptide-RNA condensates using passive microrheology with optical tweezers (pMOT). (a) A bright-field image showing a polystyrene bead (1 μm) trapped within $[KGKGG]_5$-rU40 condensates using an optical trap. Scale bar = 10 μm. **(b)** A conceptual scheme of the pMOT experiment. The bead is optically trapped within a biomolecular condensate sitting on a microscope glass surface. **(c)** Shows the 2D trajectory of the bead shown in (a) within the optical trap inside a $[KGKGG]_5$-rU40 condensate. **(d)** A plot of the normalized position autocorrelation function $A(\tau)$ of the bead motion in the X and Y dimensions in the condensate and water. **(e)** The viscoelastic moduli as obtained from normalized position autocorrelation function using equation-1 for $[KGKGG]_5$-rU40 condensates. G' and G'' represent the elastic and viscous modulus, respectively. *Inset*: frequency-dependent condensate viscosity as determined from the viscous modulus using the relation $\eta(\omega) = G''(\omega)/\omega$. **(f)** The ensemble-averaged mean square displacement (MSD) of 200 nm polystyrene beads within $[KGKGG]_5$-rU40 condensates using video particle tracking (VPT) in the absence of optical traps (see Methods section). **(g)** Comparison between the zero-shear viscosity as determined by pMOT and VPT. Error bars represent the range of the data (1% to 99%).

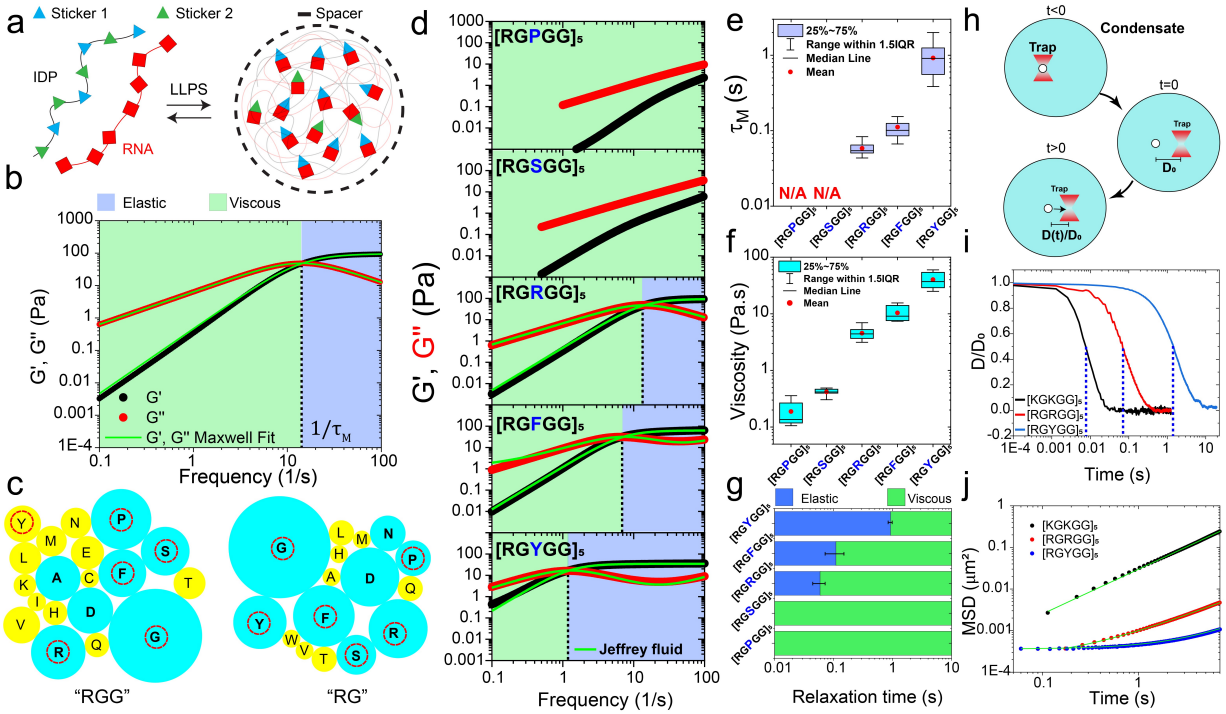

Figure 2. Sequence-dependent control over linear viscoelastic (LVE) behavior of peptide-RNA condensates. (a) A scheme showing the sticker-spacer architecture of associative peptide and RNA chains. Here, sticker-RNA interactions drive the condensation. **(b)** A plot showing the elastic modulus (G', black) and viscous modulus (G'', red) of $[RGRGG]_5$-rU40 condensate. Green lines are fits to experimental data using a single-mode Maxwell fluid model. The crossover frequency is indicated by the black dashed line and is the inverse of the terminal relaxation time τ_M. Shaded regions represent the elastic regime (light-blue) and the viscous regime (light-green). **(c)** The relative abundance of different amino acids within the inter-RG/RGG spacers of RG/RGG motifs in human RNA-binding proteins represented as bubble charts. Sizes of individual bubbles represent the fraction of inter-RG/RGG spacers that contain the corresponding amino acid (see Methods section). Residues that occurred in more than 10% of the analyzed protein sequences (RG/RGG domains from 407 human RNA-binding protein sequences) are colored cyan. **(d)** Representative plots of the frequency-dependent viscoelastic moduli of $[RG\underline{X}GG]_5$-rU40 condensates where X = P/S/R/F/Y. The crossover frequencies are indicated by black dashed lines. Shaded regions represent the elastic regime (light-blue) and the viscous regime (light-green). Green lines are fits to the experimental data using Jeffrey fluid model. **(e)** The terminal relaxation time τ_M of $[RG\underline{X}GG]_5$-rU40 condensates as measured by pMOT (X = P/S/R/F/Y). **(f)** The zero-shear viscosity of $[RG\underline{X}GG]_5$-rU40 condensates as measured by pMOT (X = P/S/R/F/Y). **(g)** An LVE state diagram indicating the time-scales at which the elastic modulus dominates (blue) and the time scales where the viscous modulus dominates (green) in $[RG\underline{X}GG]_5$-rU40 condensates (X = P/S/R/F/Y). **(h)** A scheme for the flipping trap experiment. The trap is moved instantaneously 0.3 μm to the right. The bead trajectory towards the optical trap is monitored over time. **(i)** A plot of the relative distance between the bead and the center of the trap (D/D_0) as a function of time after the trap is shifted by D_0. The bead is attracted to the trap but experiences frictional and drag forces from the condensate polymer network. Data are shown for associative condensates formed by $[KGKGG]_5$, $[RGRGG]_5$, and $[RGYGG]_5$ with rU40 RNA. Blue dashed lines indicate the time-scale at which the bead travels half the distance towards the optical trap

(D/D_0=0.5). **(j)** Mean square displacement (MSD) was measured using VPT experiments on $[KGKGG]_5$, $[RGRGG]_5$, and $[RGYGG]_5$ condensates with rU40. For $[KGKGG]_5$ and $[RGRGG]_5$, the MSD is fitted using $MSD = 4D\tau^{\alpha} + N$. For $[RGYGG]_5$, the MSD is fitted with $MSD = d^2(1 + \frac{\tau}{\tau_c})$, which is the predicted behavior for a Maxwell fluid[5].

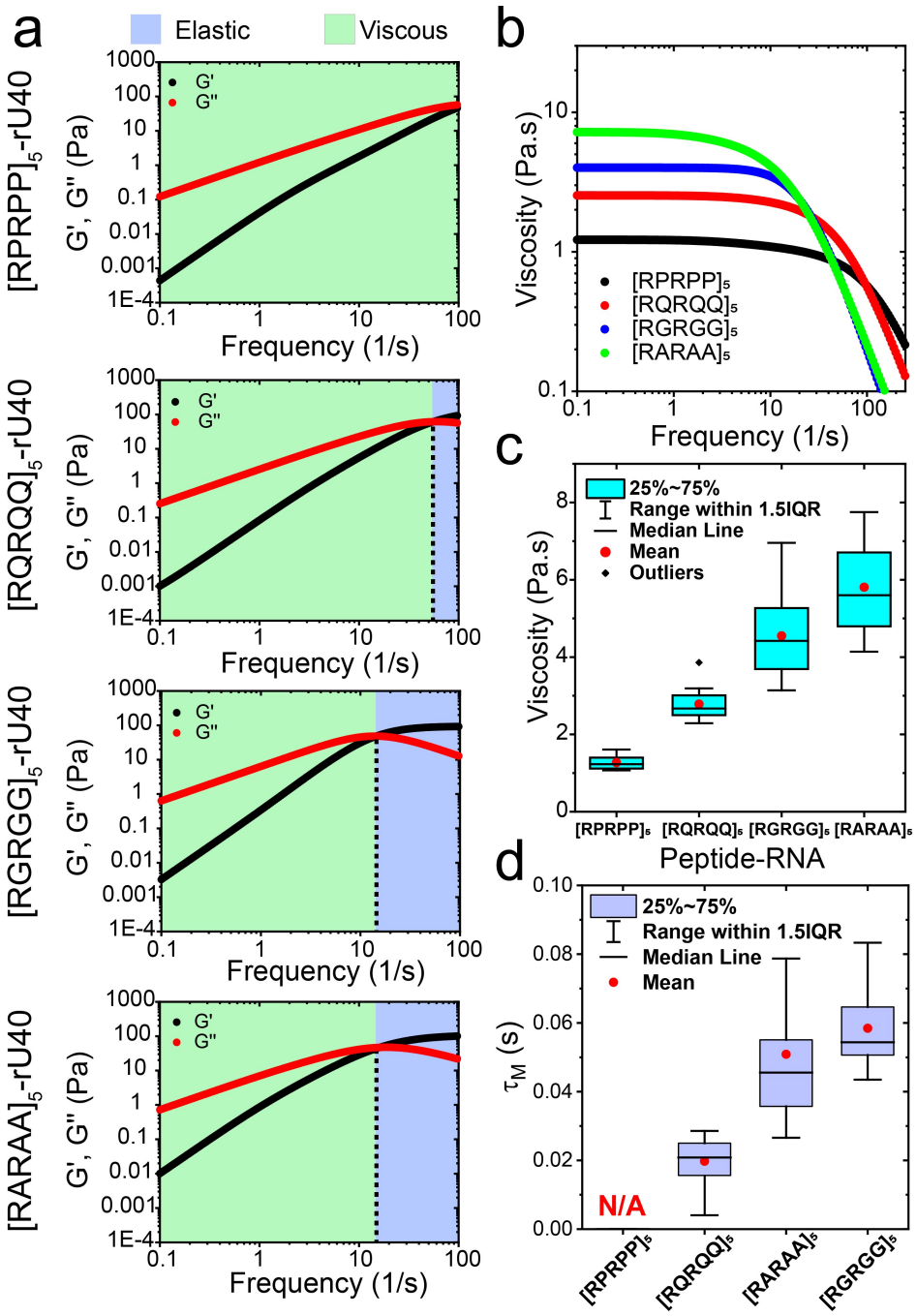

Figure 3. Effect of spacer sequence variation on the frequency-dependent viscoelasticity of peptide-RNA condensates. (a) Representative plots of the viscoelastic moduli of $[RxRxx]_5$-rU40 condensates. The crossover frequencies are indicated by black dashed lines. Shaded regions represent the elastic regime (light-blue) and the viscous regime (light-green). **(b)** The frequency-dependent viscosity of $[RxRxx]_5$-rU40 condensates as measured by pMOT. **(c)** The zero-shear viscosity of $[RxRxx]_5$-rU40 condensates as measured by pMOT. **(d)** The terminal relaxation time τ_M of $[RxRxx]_5$-rU40 condensates as measured by pMOT. For data shown in (a)-(d): x = P/Q/G/A.

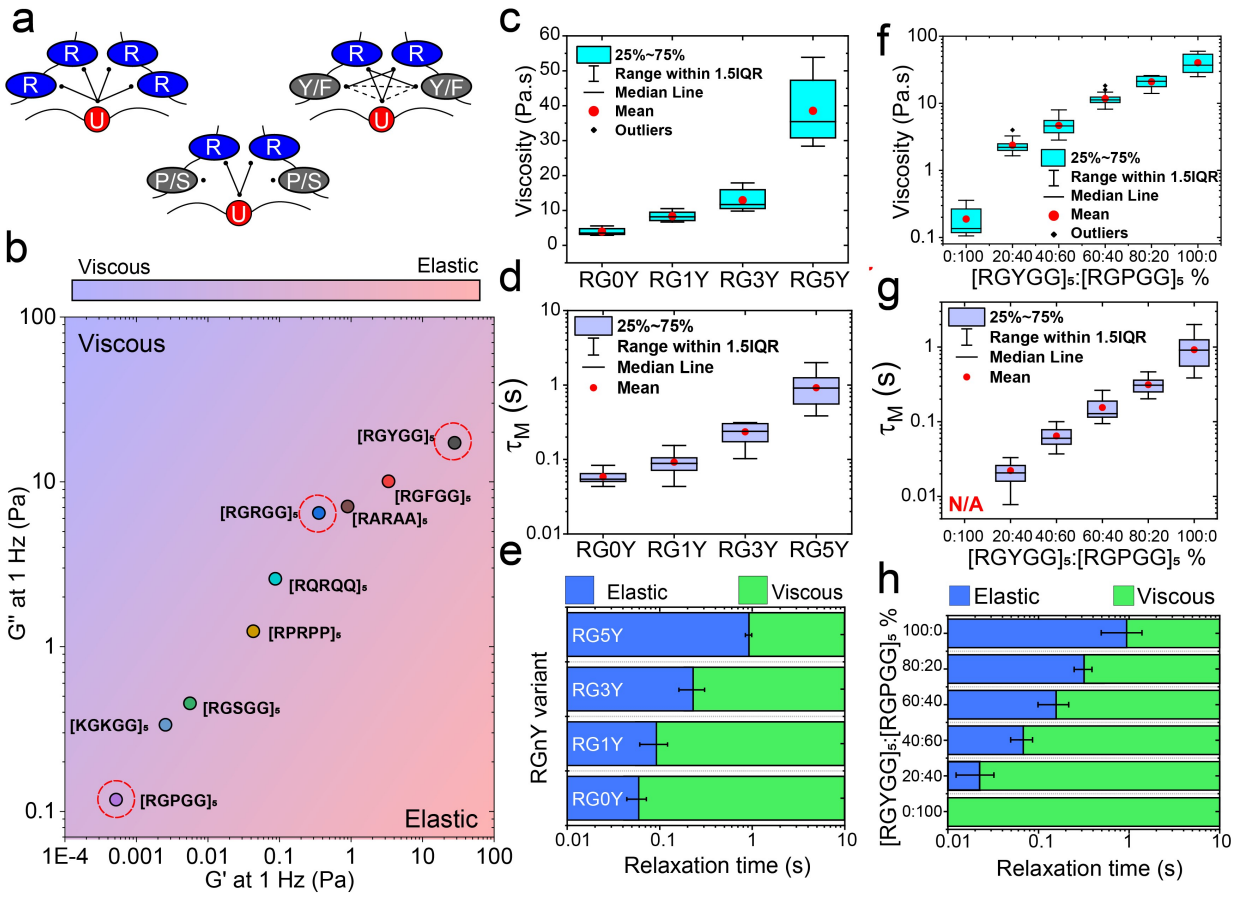

Figure 4. Continuous tuning of LVE behavior of peptide-RNA condensates by two orthogonal approaches. (a) A scheme summarizing the possible heterotypic and homotypic interactions (solid/dotted lines) between various [RGXGG]$_5$ peptides and RNA. **(b)** A plot of the elastic (G') and viscous (G'') moduli at 1 Hz frequency for the various condensate types tested in this study. This plot shows the range of tunability of the viscoelasticity of these condensates via sequence perturbations. Circles highlight the chosen sequences used for fine-tuning peptide-RNA condensate viscoelasticity: [RGRGG]$_5$, [RGYGG]$_5$, and [RGPGG]$_5$. **(c)** The zero-shear viscosity of RGnY-rU40 condensates as measured by pMOT. RGnY is defined as the [RGRGG]$_5$ peptide with n number of R-to-Y mutations at the 2nd arginine residue. RG0Y corresponds to [RGRGG]$_5$, RG5Ycorresponds to [RGYGG]$_5$ (see Table S1 and Fig. S5). **(d)** The terminal relaxation time τ_M of RGnY-rU40 condensates as measured by pMOT (see Fig. S5). **(e)** An experimental LVE state diagram indicating the time-scales at which the elastic modulus dominates (blue) and the time scales where the viscous modulus dominates (green) in RGnY-rU40 condensates. (**f-h**) Similar data as (c-e) but for condensates formed by mixtures of [RGYGG]$_5$, [RGPGG]$_5$, and RNA with variable [RGYGG]$_5$-to-[RGPGG]$_5$ ratio. Here, the total peptide concentration is fixed at 5 mg/ml and the relative fractions of [RGYGG]$_5$ and [RGPGG]$_5$ are varied. The corresponding plots of viscoelastic moduli are shown in Figure S7.

References

1 Shin, Y. & Brangwynne, C. P. Liquid phase condensation in cell physiology and disease. *Science* **357**, eaaf4382 (2017).

2 Lyon, A. S., Peeples, W. B. & Rosen, M. K. A framework for understanding the functions of biomolecular condensates across scales. *Nature Reviews Molecular Cell Biology*, 1-21 (2020).

3 Nair, S. J. *et al.* Phase separation of ligand-activated enhancers licenses cooperative chromosomal enhancer assembly. *Nature Structural & Molecular Biology* **26**, 193-203, doi:10.1038/s41594-019-0190-5 (2019).

4 Mathieu, C., Pappu, R. V. & Taylor, J. P. Beyond aggregation: Pathological phase transitions in neurodegenerative disease. *Science* **370**, 56-60 (2020).

5 Jawerth, L. *et al.* Protein condensates as aging Maxwell fluids. *Science* **370**, 1317-1323 (2020).

6 Stuart, M. A. C. *et al.* Emerging applications of stimuli-responsive polymer materials. *Nature materials* **9**, 101-113 (2010).

7 Chaudhuri, O., Cooper-White, J., Janmey, P. A., Mooney, D. J. & Shenoy, V. B. Effects of extracellular matrix viscoelasticity on cellular behaviour. *Nature* **584**, 535-546 (2020).

8 Choi, J.-M., Dar, F. & Pappu, R. V. LASSI: A lattice model for simulating phase transitions of multivalent proteins. *PLoS computational biology* **15** (2019).

9 Choi, J.-M., Holehouse, A. S. & Pappu, R. V. Physical principles underlying the complex biology of intracellular phase transitions. *Annual Review of Biophysics* **49** (2020).

10 Woodruff, J. B., Hyman, A. A. & Boke, E. Organization and function of non-dynamic biomolecular condensates. *Trends in biochemical sciences* **43**, 81-94 (2018).

11 Semenov, A. N. & Rubinstein, M. Thermoreversible Gelation in Solutions of Associative Polymers. 1. Statics. *Macromolecules* **31**, 1373-1385, doi:10.1021/ma970616h (1998).

12 Harmon, T. S., Holehouse, A. S., Rosen, M. K. & Pappu, R. V. Intrinsically disordered linkers determine the interplay between phase separation and gelation in multivalent proteins. *elife* **6**, e30294 (2017).

13 Martin, E. W. *et al.* Valence and patterning of aromatic residues determine the phase behavior of prion-like domains. *Science* **367**, 694-699 (2020).

14 Bremer, A. *et al.* Deciphering how naturally occurring sequence features impact the phase behaviors of disordered prion-like domains. *bioRxiv*, 2021.2001.2001.425046, doi:10.1101/2021.01.01.425046 (2021).

15 Jawerth, L. M. *et al.* Salt-dependent rheology and surface tension of protein condensates using optical traps. *Physical review letters* **121**, 258101 (2018).

16 Mason, T. G. & Weitz, D. A. Optical measurements of frequency-dependent linear viscoelastic moduli of complex fluids. *Physical review letters* **74**, 1250 (1995).

17 Brau, R. *et al.* Passive and active microrheology with optical tweezers. *Journal of Optics A: Pure and Applied Optics* **9**, S103 (2007).

18 Tassieri, M. *Microrheology with Optical Tweezers: Principles and Applications*. (CRC Press, 2016).

19 Preece, D. *et al.* Optical tweezers: wideband microrheology. *Journal of optics* **13**, 044022 (2011).

20 Tassieri, M., Evans, R., Warren, R. L., Bailey, N. J. & Cooper, J. M. Microrheology with optical tweezers: data analysis. *New Journal of Physics* **14**, 115032 (2012).

21 Tassieri, M. *et al.* Measuring storage and loss moduli using optical tweezers: Broadband microrheology. *Physical Review E* **81**, 026308 (2010).

22 Alshareedah, I., Thurston, G. M. & Banerjee, P. R. Quantifying Viscosity and Surface Tension of Multi-Component Protein-Nucleic Acid Condensates. *Biophysical journal*, doi:https://doi.org/10.1016/j.bpj.2021.01.005 (2021).
23 Ozdilek, B. A. *et al.* Intrinsically disordered RGG/RG domains mediate degenerate specificity in RNA binding. *Nucleic acids research* **45**, 7984-7996 (2017).
24 Thandapani, P., O'Connor, T. R., Bailey, T. L. & Richard, S. Defining the RGG/RG motif. *Molecular cell* **50**, 613-623 (2013).
25 Boeynaems, S. *et al.* Spontaneous driving forces give rise to protein− RNA condensates with coexisting phases and complex material properties. *Proceedings of the National Academy of Sciences* **116**, 7889-7898 (2019).
26 Greig, J. A. *et al.* Arginine-enriched mixed-charge domains provide cohesion for nuclear speckle condensation. *Molecular Cell* (2020).
27 Fisher, R. S. & Elbaum-Garfinkle, S. Tunable multiphase dynamics of arginine and lysine liquid condensates. *Nature communications* **11**, 1-10 (2020).
28 Chong, P. A., Vernon, R. M. & Forman-Kay, J. D. RGG/RG motif regions in RNA binding and phase separation. *Journal of molecular biology* **430**, 4650-4665 (2018).
29 Cook, K. B., Kazan, H., Zuberi, K., Morris, Q. & Hughes, T. R. RBPDB: a database of RNA-binding specificities. *Nucleic acids research* **39**, D301-D308 (2010).
30 Zhou, H.-X. Viscoelasticity of biomolecular condensates conforms to the Jeffreys model. *bioRxiv* (2020).
31 Simon, J. R., Carroll, N. J., Rubinstein, M., Chilkoti, A. & López, G. P. Programming molecular self-assembly of intrinsically disordered proteins containing sequences of low complexity. *Nature chemistry* **9**, 509 (2017).
32 Forman-Kay, J. D., Kriwacki, R. W. & Seydoux, G. Phase separation in biology and disease. *Journal of molecular biology* **430**, 4603 (2018).